

The Artificial Scientist: in-transit Machine Learning of Plasma Simulations

Jeffrey Kelling

Helmholtz-Zentrum Dresden-Rossendorf (HZDR)
Chemnitz University of Technology
Dresden, Germany
ORCID: 0000-0003-1761-2591

Vicente Bolea

Kitware Inc.
Clifton Park, NY, United States of America
ORCID: 0000-0002-5382-093X

Michael Bussmann

Helmholtz-Zentrum Dresden-Rossendorf (HZDR)
Center for Advance Systems Understanding (CASUS)
Dresden, Germany
ORCID: 0000-0002-8258-3881

Ankush Checkervarty

Helmholtz-Zentrum Dresden-Rossendorf (HZDR)
Dresden, Germany
ORCID: 0009-0004-4653-0004

Alexander Debus

Helmholtz-Zentrum Dresden-Rossendorf (HZDR)
Dresden, Germany
ORCID: 0000-0002-3844-3697

Jan Ebert

Forschungszentrum Jülich
Jülich, Germany
ORCID: 0000-0001-7118-0481

Greg Eisenhauer

Georgia Institute of Technology
Atlanta, GA, United States of America
ORCID: 0000-0002-2070-043X

Vineeth Gutta

University of Delaware
Newark, DE, United States of America
ORCID: 0000-0002-1382-8128

Stefan Kesselheim

Forschungszentrum Jülich
Jülich, Germany
ORCID: 0000-0003-0940-5752

Scott Klasky

Oak Ridge National Laboratory
Oak Ridge, TN, United States of America
ORCID: 0000-0003-3559-5772

Richard Pausch

Helmholtz-Zentrum Dresden-Rossendorf (HZDR)
Dresden, Germany
ORCID: 0000-0001-7990-9564

Norbert Podhorszki

Oak Ridge National Laboratory
Oak Ridge, TN, United States of America
ORCID: 0000-0001-9647-542X

Franz Pöschel

Center for Advance Systems Understanding (CASUS)
Görlitz, Germany
ORCID: 0000-0001-7042-5088

David Rogers

Oak Ridge National Laboratory
Oak Ridge, TN, United States of America
ORCID: 0000-0002-5187-1768

Jeyhun Rustamov

Helmholtz-Zentrum Dresden-Rossendorf (HZDR)
Dresden, Germany
ORCID: 0000-0002-4803-2461

Steve Schmerler

Helmholtz-Zentrum Dresden-Rossendorf (HZDR)
Dresden, Germany
ORCID: 0000-0003-1354-0578

Ulrich Schramm

Helmholtz-Zentrum Dresden-Rossendorf (HZDR)
Dresden, Germany
ORCID: 0000-0003-0390-7671

Klaus Steiniger

Helmholtz-Zentrum Dresden-Rossendorf (HZDR)
Center for Advance Systems Understanding (CASUS)
Dresden, Germany
ORCID: 0000-0001-8965-1149

René Widera

Helmholtz-Zentrum Dresden-Rossendorf (HZDR)
Dresden, Germany
ORCID: 0000-0003-1642-0459

Anna Willmann

Helmholtz-Zentrum Dresden-Rossendorf (HZDR)
Dresden, Germany
ORCID: 0009-0001-9992-6027

Sunita Chandrasekaran

University of Delaware
Newark, DE, United States of America
ORCID: 0000-0002-3560-9428

Abstract—Large-scale simulations or scientific experiments produce petabytes of data per run. This poses massive challenges for I/O and storage when scientific analysis workflows are run manually offline. Unsupervised deep learning-based techniques to extract patterns and non-linear relations from these large amounts of data provide a way to build scientific understanding from raw data, reducing the need for manual pre-selection of analysis steps, but require exascale compute and memory to process the full dataset available. In this paper, we demonstrate a heterogeneous streaming workflow in which plasma simulation data is streamed directly to a Machine Learning (ML) application training a model on the simulation data in-transit, completely circumventing the capacity-constrained filesystem bottleneck. This workflow employs openPMD to provide a high level interface to describe scientific data and also uses ADIOS2, to transfer volumes of data that exceed the capabilities of the filesystem. We employ experience replay to avoid catastrophic forgetting in learning from this non-steady state process in a continual manner and adapt it to improve model convergence while learning in-transit. As a proof-of-concept we approach the ill-posed inverse problem of predicting particle dynamics from radiation in a particle-in-cell (PICongPU) simulation of the Kelvin-Helmholtz instability (KHI). We detail hardware-software co-design challenges as we scale PICongPU to full Frontier, the Top-1 system as of June 2024 Top500 list.

Index Terms—Exascale Computing, Computer architecture, High Performance Computing, Plasma simulations, In-memory computing, Data-driven modeling, Unsupervised learning, Dimensionality reduction

I. INTRODUCTION

HPC simulations capable of fully exploiting the compute power of supercomputers produce a wealth of high quality, complex data. Examples for such simulations include digital twins of the earth, whole device models of magnetic fusion reactors or simulations of advanced particle accelerators. The data rates and volumes of such simulations can be compared to instruments at large-scale research infrastructures such as tomography endstations at synchrotrons in photon science, high energy physics experiments, fusion research facilities or astro-particle observatories [1].

Exploiting such a huge volume of data optimally often focuses on fast data selection including data filtering, triggering, anomaly and outlier detection or intelligent data reduction. In-situ inference using pre-trained machine learning (ML) models has led to a broad inclusion of such techniques across scientific communities [2]–[5].

Here we want to highlight an open challenge, namely the situation in which the stream of data produced by a simulation or any other source such as a scientific instrument remains at such a scale and quality that data reduction still demands in-transit analysis. In such cases, even if the volume of data is reduced to the minimum extent suitable for analysis, storage of such data for further offline analysis is impossible due to the physical constraints of the filesystem at hand.

The open challenge in our case is a particle-in-cell simulation of a Kelvin-Helmholtz instability (KHI) [8] as shown in Fig. 1 (more details in Section II). Instabilities are one of the most fundamental yet complex collective phenomena in plasma physics. Their growth rate, scale lengths and dynamics

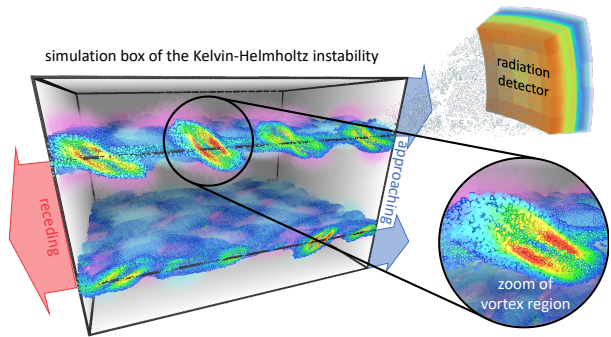


Fig. 1: 3D rendering of the KHI simulated with PICongPU [6] and rendered with ISAAC [7]. The middle graphic shows electrons as particles that radiate strongly, with the radiation intensity indicated from blue to red. The initial plasma flow direction is depicted as arrows, blue marking propagation towards and red away from the radiation detector. The spectrally resolved radiation determined by the synthetic radiation detector is illustrated for a finite solid angle, showing radiation intensity per direction and frequency (indicated by depth).

show a strong non-linear dependence on the plasma properties. Understanding and controlling instabilities is critical across all disciplines of plasma physics from magnetic and inertial fusion to space physics, plasma acceleration or astrophysics. Ultimately, reconstructing the complete phase space dynamics of a plasma from observations would provide us with the most detailed view of the growth and dynamics of instabilities and thus on the most central plasma properties at high temporal and spatial detail.

Reconstructing the complete phase space dynamics of a plasma requires processing of a wealth of information. One of the most challenging use cases in this class of problems is the in-transit training of data-driven complex machine learning models at extreme data rates, where training the model requires most of the data produced by the source. The model being trained itself is of such complexity that it can in principle incorporate the complexity of the total volume of data produced by the source, while at no time a total view of the data is available.

We note that a large number of advances in ML rely on iterative training [9], where the model repeatedly learns from the input data over multiple epochs, requiring permanent storage of the datasets. In the reference case studied in our work, this is not the case, as data is produced on demand and discarded after being used for training. We thus have chosen a continuous learning approach to address this challenge. Although methods for continuous learning exist [10], they have not had to consider the time constraints imposed by the speed of data generated from simulations [11]. Thus, adapting the continuous learning techniques to handle such constraints is a critical challenge in the field of ML for high rate streaming of scientific data.

The other challenge is to effectively navigate the memory hierarchy of heterogeneous computing systems, as it exposes enormous differences in throughput [12], [13]. While internal throughput in GPUs can easily reach the TB/s range on a single

node, breaking down the throughput of massively parallel filesystems to the single node throughput reveals maximum performance of several tens of MB/s only. Each node often houses more than one GPU, hence available data storage and bandwidth demand data reduction, often done by discarding highly valuable data in practice.

We further note that the mismatch in throughput between memory hierarchies in modern HPC systems has been steadily growing, increasing the number of cases in which offline analysis is impossible and thus the urgency to find solutions for online analysis of data at high rates and volumes [12]. We argue that in case of such extreme rates online analysis of streaming data is the method of choice [7], [14], reducing the overall amount of data that needs to be stored while using computationally demanding algorithms to make optimum use of the data produced. However, this means that a complete view of all data produced is never available at any time of the analysis workflow and there is a need to preserve the extreme data throughput during the whole analytics pipeline.

In our work we showcase a real-world example and present a general solution that implements all relevant parts of online in-situ training of a large-scale model on the Frontier exascale supercomputer at ORNL [15]. We argue that the building blocks of our solution are general enough to be adapted to almost any use case of the type discussed above with only minor adjustments. We furthermore emphasize that besides presenting a full workflow, the additional unique value of this work is to highlight the multi-parameter optimization problem of fitting the available compute and data transfer resources to achieve the best result in the shortest amount of time. We remark that our technique is especially interesting in the case of irreversible data loss [16], and thus extends well beyond the case of large-scale simulations as high rate data sources presented here.

With a goal to automatically extract knowledge from large scale simulations, the paper makes the following contributions:

- **Computationally:** We present a workflow that integrates a particle-in-cell simulation of the Kelvin-Helmholtz instability (KHI), supported by openPMD-streaming [14], with a PyTorch [17]-based ML application (*which we refer to as MLapp from here on*). We regard this orchestration as the *Artificial Scientist*. This orchestration, to the best of our knowledge, is the first of its kind.
- **Scientifically:** We uncover correlations between emitted radiation and particle dynamics within the simulation in an unsupervised manner to create an inverse map from the observed radiation to the particle dynamics and to identify the aspects of the particle dynamics that are relevant to the remotely observable radiation signatures of KHI.
- Using lessons learned from this orchestration and challenges faced, we provide input on what needs to be improved as we attempt to understand complex scientific data generated by instruments.

II. THE RELATIVISTIC KELVIN-HELMHOLTZ INSTABILITY

The Kelvin-Helmholtz instability (KHI) is a well-known shear surface instability observed in plasmas [8]. It is driven by a self-amplifying cycle of small density or velocity fluctuations that lead to a growing magnetic field at the shear surface, which further amplifies the initial fluctuations as depicted in Fig. 1. This phenomenon occurs in astrophysical scenarios, including Saturn’s magnetopause [18], but also in fusion reactors and inertial confinement fusion (ICF) [19], [20]. While the theoretical understanding and simulation capabilities of KHI [21], [22] are well established, direct measurement of the predicted density changes remains a real challenge. Because of its well-understood dynamics, we chose KHI as a test case for our study to validate the results of our orchestrated workflow against existing knowledge.

A promising approach to the analysis of plasma dynamics is the study of the emitted radiation, which provides valuable information about the plasma properties and has been successfully applied in previous studies of the KHI [23]. However, this correlation process typically requires extensive post-processing and analysis, often spanning several years.

Here, we simulate the KHI using the plasma simulation code PIConGPU [6], [24] which utilizes the alpaka library [25] for performance portability and has been at the forefront of developing central technologies for GPU-accelerated plasma simulations. It was the first particle-in-cell (PIC) [26] code to run performant simulations on a variety of architectures in the world over many years [7].

III. RECONSTRUCTING THE LOCAL PHASE SPACE DYNAMICS OF THE RELATIVISTIC KHI FROM OBSERVABLE RADIATION

In this section, we will showcase the challenges faced and solutions employed to solve an extreme-scale inverse problem via a complex HPC workflow coupling a GPU-accelerated plasma simulation (KHI/PIConGPU) to a large-scale in-situ neural network for in-situ learning. This workflow as a whole, is a novel approach, to the best of our knowledge.

Fig. 2 depicts the interrelations between observational data, such as radiation, and simulation state, such as particles, as both inputs and outputs to data-driven models. Our objective of approximating the inverse mapping from observed radiation to particle dynamics can abstractly be described by the information flow depicted in Fig. 2(a). For the model to remain tractable a reduced representation of the complex particle dynamics is required, which is learned by an auto-encoding model Fig. 2(b). To observe the extent to which this representation captures relevant features of the particle dynamics, it is worthwhile to train a surrogate model of the, computationally expensive, forward process of radiation emission (Fig. 2(c)). These three tasks integrate into our ML model, described later, also in Fig. 7.

It was shown in 2013 [6] that the computation of high quality, high resolution observational data such as radiation spectra can only be performed in-situ, as storing the ground truth data, the phase space trajectory data of each particle

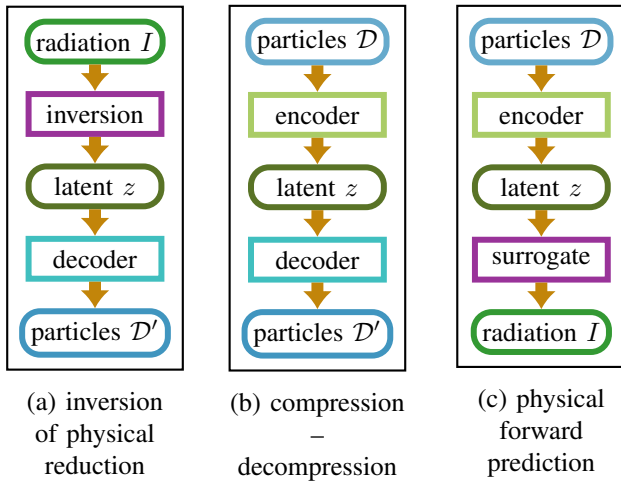


Fig. 2: Tasks an ML model can be trained on based on simulation data in-transit. Rounded boxes (\circ) indicate inputs/outputs, sharp boxes (\square) represent neural networks. Same colors mark same data types/neural nets. – (a) solving the inverse problem of predicting particle dynamics from radiation signatures; (b) extracting features of particle dynamics and reconstruction thereof (representation learning/compression); (c) surrogate model of radiation emitted by complex particle dynamics.

in the simulation at each time step, is impossible due to the aforementioned throughput hierarchy. As an example, scaling to a moderate 25 % of the Frontier system, one would be faced with 1 PB of data for every time step. With total time steps per simulation of the order of a few thousand time steps and time step durations of the order of 0.1 to 1 s, we frequently observe data rates of 1 to 10 PB/s for particle trajectory data and theoretically require total volumes on disk of the order of 10 EB. Depleting storage in as little as 100 s. We thus end up with the conundrum to employ data-driven models for solving a large-scale ill-posed inverse problem.

A. A complex in-memory workflow to reconstruct local phase space dynamics from radiation

A particular challenge for the reconstruction of local phase space dynamics is that their radiation signatures are highly convoluted, composite quantities that combine multiple facets of the ground truth which to restore. This observation guides our approach at learning from a live PIC simulation, as the posed problem is now diagnosed as ill-posed. In detail, the observed radiation spectrum is both spectrally and angularly resolved and the observed intensity at each wavelength and direction varies between time steps according to the changes of the phase space dynamics. The observed intensity in each direction and at each wavelength is a weighted sum of all contributions from all particles.

Hence here are the steps to be taken:

- Simulate a sufficiently large domain at high spatial and temporal resolution to capture both the local plasma dynamics as well as the collective contributions of different plasma regions to the total radiation spectrum.

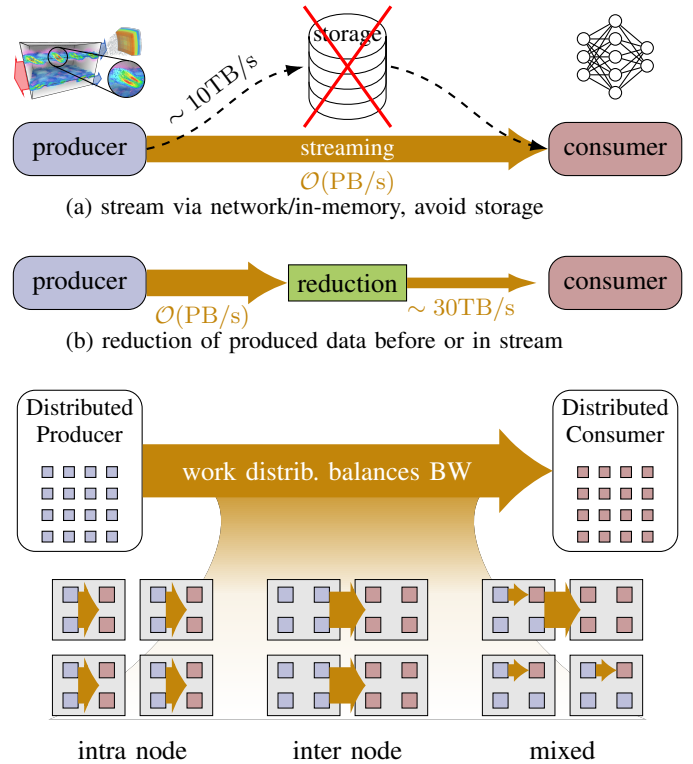


Fig. 3: Three aspects to streaming between loosely coupled producer and consumer: (a) streaming without going through storage unlocks more bandwidth; (b) reducing simulation data close to the producer lowers bandwidth requirements; (c) to distributed producer and consumer, system topology presents communication paths with vastly different bandwidths which must be reconciled with the loosely-coupled application's communication requirements.

- At each PIConGPU time step:
 - Calculate the radiation spectrum directly in-situ as the sum of the contributions from all radiating particles in the simulation at each time step, with high angular and spectral resolution and bandwidth.
 - Collect the particle phase space data, positions and momenta, and the complex amplitude and phase for each wavelength and direction of the radiation.
 - Prepare the collected data for an ML model by finding a suitable encodings for spectral and phase space data.
 - Stream that data to an ML model and asynchronously train the model.
- Stop the simulation after observing the complete physical process under investigation.

B. The technical challenge: Exascale data streaming and continual learning

An important design goal for the implementation of the above data processing scheme is to **write no simulation data** to the filesystem during the entire workflow. File I/O can

certainly be initiated when desired, but is independent of and not necessary for the workflow.

While **in-situ** approaches have been previously used to compute scientifically relevant analyses through plugins within the same application context [6], this is no longer possible for the envisioned ML analysis, as the vastly incompatible software stacks for the C++ simulation code PIConGPU and the PyTorch-based MLapp as well as their different scaling properties inhibit such an integration into a **strongly-coupled** monolithic application framework. Hence, simulation and the MLapp are modularized into two separate applications that communicate through a standardized data interface, a pattern that we refer to as **loose coupling**, since the standardized data interface allows to plug together a data processing pipeline more flexibly, i.e. loosely than before. When the implementation for such workflows avoids writing intermediate data to disk, we refer to them as **in-memory**. In-memory workflows include such setups where data is not moved, staying within one application’s memory (**in-situ**), and alternatively setups that move data from one into another application’s memory (**in-transit**) (Fig. 3(a)). The latter becomes necessary when transitioning from file-based workflows to in-memory workflows without sacrificing flexibility in the data exchange pattern, as well as in response to codes that scale differently.

The whole simulation, all data produced by the simulation and ingested by the model, and the whole model all reside in-memory and data is distributed and optionally reduced in-transit (Fig. 3(b)).

The physical workflow outlined in III-A can be directly translated into a technical setup that is the main subject of this work:

- Start a scalable, GPU-accelerated PIConGPU simulation of sufficient size and resolution, utilizing a large subset of nodes on Frontier.
- Schedule PyTorch and N/RCCL alongside the PIConGPU simulation. (N/RCCL - NVIDIA and ROCm collective communication library)
- Optimize scheduling for data transport and locality, physical system size and resolution, simulation and training time, total time of solution and use of resources (options in Fig. 3(c)).
- At each simulation time step
 - stream particle momenta and positions and spectral data to a large-scale ML model,
 - transform the phase space and spectral data from its simulation format to an optimum format for the ML mode and
 - train the model concurrently.
- Repeat the workflow for a sufficient number of time steps to cover all relevant stages of the plasma instability simulation with respect to the dynamical evolution and amount of training data needed.

For supporting an online workflow which stores no intermediate data such as phase space trajectory and radiation data to disk, the model must be continuously trained online from

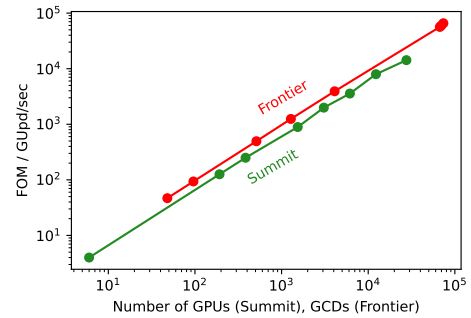


Fig. 4: FOM scaling of PIConGPU from 24 GPUs (6 nodes) to 36 864 GPUs (9216 nodes) on Frontier (red line) using a general test case [27]. PIConGPU achieves an average FOM for the largest run of 65.3 TeraUpdates/s vs 14.7 TeraUpdates/s on Summit.

the series of time step data. This requires the model to be trained by subsequent snapshots of the evolution of plasma and radiation data. For this, continual learning is the methodology of choice as outlined in Section IV-C.

We strongly believe that a large class of inversion problems for complex, large-scale systems that produce data streams face similar challenges and that our solution presented here for the first time introduces all relevant building blocks and technologies to address these challenges.

IV. METHODOLOGY

A. Particle-in-cell simulation and its setup

To simulate KHI, we employ the fully kinetic 3D3V relativistic particle-in-cell (PIC) method [26] using the open-source code PIConGPU [6], [24]. The PIC method iteratively models plasma dynamics by advancing particle positions and velocities in response to electromagnetic forces, while the electromagnetic fields are updated based on the electric current caused by the particle motion.

For modeling the KHI with PIConGPU, the smallest volume we simulate is $192 \times 256 \times 12$ cells on 16 AMD MI250X GPUs using cubic cells of $\Delta x = 93.5 \mu\text{m}$ and a time step duration of $\Delta t = 17.9\text{fs}$ at a particle density of $n_0 = 10^{25} \text{m}^{-3}$. We initialize two counterpropagating plasma streams (as shown in Fig. 1) with a normalized velocity of $\beta = \frac{v}{c} = 0.2$ and initialize 9 particles per cell.

To prove that PIConGPU can scale on a large system for general plasma physics cases, we use a more challenging test case [27] than the KHI as a scaling benchmark, with a higher particle-per-cell ratio. Fig. 4 shows scaling runs on ORNL’s Summit and Frontier.

On Frontier with a total of 36 864 AMD MI250X GPUs across 9216 nodes [28], a scaling of PIConGPU’s Figure of Merit (FOM), i.e. the weighted sum of the total number of particle updates per second (90%) and the number of cell updates per second (10%), is demonstrated as shown in the weak scaling results. In this particular configuration, the simulation included $2.7 \cdot 10^{13}$ macroparticles in 10^{12} grid cells, compared to our base FOM run on Summit in 2019, where only $1 \cdot 10^{13}$ macroparticles in $4 \cdot 10^{11}$ cells could be used.

On Frontier, one thousand time-steps completed in a mere 6.5 minutes. This is due to several factors. Spatial domain decomposition distributes computational domains across GPUs and computers, exploiting data locality and enabling parallelization. Efficient data structures, such as supercells in PIConGPU [29], optimize data access patterns within these domains, while asynchronous communication strategies between compute nodes minimize communication overhead when exchanging information between different domains. In addition, usage of the libraries PMac [30] and alpaka [25] abstract data management and hardware-specific optimizations, enabling portability across architectures.

PIConGPU uses openPMD [31], [32] to output data. By using openPMD, we stream particle data in-transit via ADIOS2 [33] (*see Section IV-B*) directly to the ML framework, thus avoiding filesystem limitations [12]. In addition, PIConGPU supports strongly-coupled in-situ processing and analysis methods, among which we use the far-field radiation plugin for our study. In contrast to the intrinsic field solver, the far-field radiation plugin [34] calculates radiation emissions using the Liénard-Wiechert potential approach [35], thus overcoming common limitation of the PIC algorithm, as it resolves much higher frequencies, directly predict observable spectra, and correctly quantify coherent and incoherent radiation [36]. However, it comes at a high computational cost, scaling with the number of particles, frequencies, and directions, easily exceeding the computational limits of the underlying particle-in-cell simulation [37].

Since the computational cost of the far-field radiation plugin can be significant, forward calculations can become prohibitively expensive for a wide range of simulation parameters. Furthermore, inversion from observed radiation back to particle dynamics remains a challenging task, requiring ML-based innovative approaches. Thus, we implemented a novel ML approach (*see Section IV-C*) that was trained on both particle distributions and their associated radiation using streamed data from PIConGPU. After training, the ML model should generate particle distributions based on the input spectra, providing a potential solution to the inversion problem and improving our ability to interpret plasma dynamics based on observable radiation.

B. Data streaming via openPMD

Considering that PIConGPU as well as the MLapp both rely significantly on very different software stacks, launching both parts of the setup in the same application context is not feasible. As detailed previously in III-B, we follow a loose-coupling rather than a tight-coupling approach [14], launching both applications separately. Output created by PIConGPU must be moved across the application boundary to the MLapp, without impacting the scalability of the setup through use of limited resources such as the parallel filesystem. The solution pursued in this paper is an **in-transit** workflow that keeps data in memory at all times and writes no intermediate data to disk.

The in-transit I/O solution is put in place by openPMD [31] implemented within PIConGPU and the MLapp.

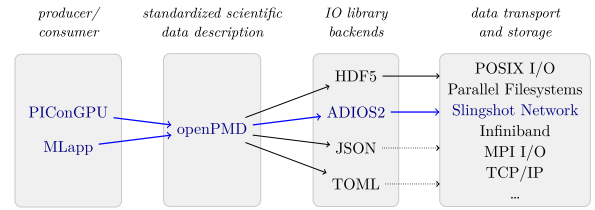


Fig. 5: High-level overview of the software stack for data exchange between PIConGPU and the MLapp.

openPMD [32] is a data standard for particle-mesh data built for F.A.I.R. scientific I/O in HPC software that needs to scale, and it is employed in a diverse ecosystem of simulation, analysis and visualization codes [38]. In turn, the I/O building block for the orchestration of the *Artificial Scientistis* modular and generically reusable for other setups of this kind.

As an open *data* format, openPMD can be implemented in various *file* formats such as JSON, TOML, HDF5 and ADIOS2, all supported by the reference implementation openPMD-api, of which we further consider ADIOS2 in this study due to its support for in-transit I/O in HPC settings, as shown in Fig. 5. This flexible choice of backends for scalable and quickly adaptable I/O solutions gains outstanding relevance on exascale like Frontier where even modern solutions for classical I/O via parallel filesystems, e.g. the provisioned Orion filesystem, cannot be expected to scale up to full system size as a base for a loosely coupled data analysis pipeline.

The in-transit data strategy is built upon the Sustainable Staging Transport (SST) [39], [40] data engine of ADIOS2 that connects one parallel data producer code to an arbitrary number of parallel data consumer codes, hereby opening connections only between processes that actually share data. For adapting to different system architectures, the SST engine implements different network transport technologies (*data planes*), including TCP (non-scalable fallback), libfabric, ucx and the `MPI_Open_port()` API of MPI. For this benchmark, we consider the low-level libfabric data plane on top of the system’s CXI provider [41] which allows, yet also requires more manual finetuning, as well the MPI data plane which leverages the MPI implementation’s performance tuning.

The use of HPC interconnects such as the Slingshot network on Frontier or Infiniband on e.g. Summit is an important cornerstone in the general applicability of this I/O building block, since this I/O approach thus retains the flexibility of setups based on the parallel filesystem. In particular, there is no lock-in to a specific pattern for data exchange, compared to approaches based on e.g. local SSDs or shared memory. While local data exchange within a node remains preferred for scalability, this I/O approach naturally extends towards patterns such as staging within a neighborhood of nodes (for scheduling reasons or for implicit load balancing via streaming) or a fan-in pattern (for data reduction purposes), both of which are potential directions to pursue.

Before applying this I/O solution to the MLapp, we demonstrate its scalability to the full system using a synthetic benchmark that runs PIConGPU’s KHI scenario full-scale and

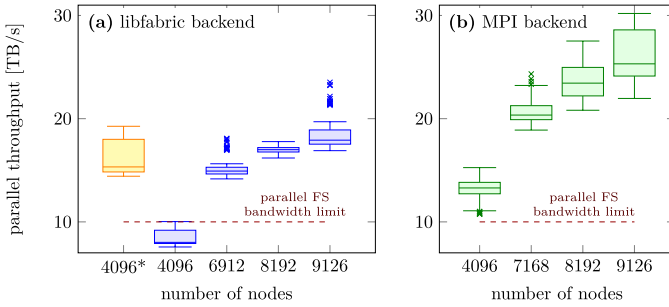


Fig. 6: Parallel total throughput for streaming at full scale on Frontier using a synthetic benchmark built on PIconGPU KHI. An obvious outlier result was removed for the libfabric backend at 8192 nodes. (a) Using the libfabric data plane and the CXI provider to access the Slingshot network at a lower level. (b) Using the MPI data plane based on `MPI_Open_port()`. The perceived parallel throughput reaches around 20TB/s for libfabric, and from 20 - 30 TB/s for MPI.

streams its particle data into a synthetic no-op consumer that performs no computation beside measuring the performance of this I/O operation and only discards received data. Employing the no-op consumer gives us a testbed for full-system scaling runs of a particle data stream fed by PIconGPU, helping us identify and eliminate scaling issues before applying the full PIconGPU+MLapp pipeline. In that context, the major challenge is to scale to a large number of parallel instances, while the amount of data streamed per instance comes as a secondary scaling target.

The PIconGPU KHI simulation is run from half (4096 compute nodes) to full-scale (9126 compute nodes) of Frontier, producing 5.86 GB of particle data per compute node and time step. Fig. 3(c) (bottom left) shows the processes running within each compute node and the data flow between them. At each scaling run (weak scaling), five time steps are sent from PIconGPU to the no-op consumer, which then measures the time needed for loading the data. The perceived parallel throughput is computed based on this measured time and the global data size, i.e. the previously mentioned 5.86 GB per node multiplied with the number of nodes. While including communication overhead, this perceived parallel throughput has been shown in [40] to be a close approximation for the real throughput in this kind of setup.

The benchmarks in Fig. 6 demonstrate the feasibility of this I/O strategy for full-scale workflows. Depicted are boxplots of all single measurements. Most notably, we observe a maximum perceived parallel throughput of 20 - 30 TB/s which compares outstandingly against the 10 TB/s bandwidth of the parallel Orion filesystem, a scaling limit which we circumvent and exceed by not using the filesystem for intermediate data. Furthermore, these results can also compare well against the 35 TB/s aggregate write bandwidth of the SSDs installed locally in the compute nodes [42].

For the libfabric-based benchmarks, we initially used an implementation that enqueued all read operations to the network at once and waited for replies (labeled 4096* in Fig. 6). While these results signify the best achieved per-node throughput

of 3.5 - 4.7 GB/s at 4096 compute nodes (*a total of 14.1 - 18.8 TB/s*), it turned out that this strategy did not scale to the full system, so we employed an alternative that enqueued operations in batches of 10 operations. While this turned out to scale to the full system, it came at a notable cost in performance, visible in a per-node throughput of 1.9 - 2.6 GB/s at 9126 compute nodes (*a total of 16.5 - 23.0 TB/s*). Conversely, the MPI data plane yields a per-node throughput from 2.6 - 3.7 GB/s at 4096 compute nodes (*a total of 10.5 - 14.9 TB/s*) to 2.4 - 3.3 GB/s at 9126 nodes (*a total of 21.4 - 29.5 TB/s*), **the best achieved system-wide parallel throughput** from this experiment.

We conclude that the MPI data plane brings default good performance, while the libfabric data plane’s lower-level control can bring performance improvements but at the cost of necessary fine-tuning beyond this study’s scope. Since only a single instance of the reader code was running per node, its throughput (1.9 - 4.7 GB/s, across all cases) compares against the max possible throughput of a single HPE Slingshot NIC at 25 GB/s. This implies that further speedup can be achieved by parallelizing the reader in the actual PIconGPU+MLapp pipeline. The benchmarks suggest that the MPI data plane be used, which can be explained by leveraging system-specific performance tuning in the MPI implementation. All regular measurements range between 1.2 s - 3.2 s.

C. Machine learning

The task of in-transit ML is to extract patterns from the live observations and thereby learn correlations between variables and reduced representations. Here, we focus on predicting particle dynamics from radiation spectra, which constitutes an ill-posed problem in that any given radiation spectrum can potentially be produced by various types of dynamics. When learning in-transit from a simulation, this problem is reduced from an intractable general case to the question of: which type of local particle dynamics under the given physical setup, i.e. the relativistic KHI, gave rise to an observed radiation spectrum observed in one direction, which, however, remains an ill-posed problem. Many ML techniques, especially feed-forward networks, tend to predict the mean of possible inversions, even if this itself is not a valid solution [43]. One class of techniques specifically designed to learn by sampling from conditional multi-modal distributions, such as those that occur as solutions to our ill-posed problem, are flow-based models [44], [45] and invertible neural networks (INNs) [46]. These learn an invertible transformation, or change-of-variables, between a chosen posterior distribution, often a normal distribution \mathcal{N} , and a prior described by the training data, in our case the distribution of observed particle dynamics \mathcal{D} . One specific difference between them is, that INNs also learn the deterministic forward function defining the inverse problem, in our case the mapping between samples of particle dynamics \mathcal{D} and radiation spectrum I . Put differently, they also learn to predict the condition I under which a given sample of the prior D may occur.

Particle configurations in phase space of the plasma dynamics simulated here can be very complex, such that a small sample of particles cannot adequately represent the dynamics. For INNs and flow-based models this poses a challenge, because the change-of-variables approach [47], [48] dictates, that the information volume, i.e. the number of activations at the input and output of each coupling block, must be constant throughout the network, which results in a very large network when working with a prior distribution of dimensionality on the order of 10^5 . In this setting, the number of network parameters can be kept in check by using affine flows [44], [49] with designed convolutional sub-networks which should also be invariant to transposition of particles in the input vector to be efficiently trainable.

When generating point cloud (PC), flow-based models are typically tasked with sampling them point-by-point, i.e. the model learns a probability density that describes the particle density in phase space. The main drawback here is, that the model has to learn the many-modal distributions which can occur in the KHI phase space on a single-particle basis and can not longer generate multiple particle distribution for a single condition, i.e. not distinctly produce all PCs solving an ill-posed problem. Another issue is, that, unless we use an encoder (conditioning network) producing very small latent vectors of around six dimensions for the radiation, the dimension of the condition \mathcal{I} is much larger than the dimension of the prior while the network has to be sampled $\mathcal{O}(10^3)$ times to retrieve a useful particle distribution.

To overcome the above inefficiencies, we opted to view the particle configuration as a point cloud (PC) and reduce the dimensionality of the prior \mathcal{D} by tasking an outer network to learn latent representations of the phase space, which are also invariant with respect to transposition of particles. This outer network can in principle be an autoencoder (AE) whose latent representation z is passed to the INN as the prior \mathcal{Z} . In practice, the INN will not generate exact latent vectors z' on its backward pass, but variations, which will cause the AE's decoder to fail at reconstruction. Therefore, we employ a variational auto encoder (VAE) instead, which, albeit harder to train, intrinsically trains its decoder to be robust against the variations produced by the INN.

As depicted in Fig. 7, there are three main blocks of the network architecture:

- The encoder (light green) follows an architecture proposed in [50], which by itself is a simplified version of PointNet [51], using 1×1 convolutions acting on the coordinates of $3 \cdot 10^4$ particles separately to gradually (channels: $6 \rightarrow 16 \rightarrow 32 \rightarrow 64 \rightarrow 128 \rightarrow 256 \rightarrow 608$) extract 608 features per particle, followed by a max-pooling to obtain a transposition-invariant feature set, which is then processed by two multi-layer perceptrons (MLP), each with $\rightarrow 608 \rightarrow 544$ hidden features, to obtain predictions for the mean μ and standard deviation σ to sample the 544-dimensional latent vector z .
- The decoder (cyan) uses a single fully-connected layer ($\rightarrow 1024$, reshaped to $(2, 2, 2, 16)$) to transform the latent

z before using 3D deconvolutions (channels: $16 \rightarrow 8 \rightarrow 6$, kernelsize: 2^3 , stride 2^3) to upsample to 4096 particles. While generating a larger PC that matches the input size of 30 000 particles would be beneficial to obtain a smoother loss surface, training a network that generates only 4096 particles as output is also feasible and will reduce the VAE network size. In the present case, using 30 000 particles as an input during training, the network can learn to generate important particles to represent the target PC. Randomly sampling fewer particles from the input would not yield a sufficient representation.

- The INN for the inverse mapping (violet) is built from four Glow coupling blocks [52] using MLPs with $\rightarrow 272 \rightarrow 256 \rightarrow 544$ hidden layers as subnets. The hidden layer sizes were chosen to form a bottleneck and reduce to a computationally efficient power of two.

The loss function to be minimized during training of this architecture consists of five terms, two connected to the VAE and three for the INN, detailed below:

- As the reconstruction loss of the VAE, we use Chamfer's distance (CD) [53], which is the most commonly used differentiable function to compare PCs in literature, because it is efficient to compute.
- Regularization of the VAE's latent space is controlled by Kullback-Leibler divergence (KL) [54].
- The resulting spectrum I' of the INNs forward function is compared to the ground truth using mean-squared error $\text{MSE}(I', I)$
- The posterior normal distribution, produced by the INN's forward pass, and the prior distribution, produced by the INN's backward pass, are both evaluated using maximum mean discrepancy (MMD) using an inverse multi-quadratic kernel, as proposed in [46].

The total loss corresponds to the weighted sum

$$L = 1 L_{\text{EMD}} + 0.001 L_{\text{KL}} + 0.1 (3 L^2 + 400 L_{\text{MMD}(z, z')}) + 0.3 L_{\text{MMD}(\mathcal{N}, \mathcal{N}')} \quad (1)$$

The numerical values for the coefficients were empirically tuned to optimize performance of the AE reconstruction and the INN forward and backward predictions.

While training on the continuous data stream of non-steady configurations, we employ experience replay (EP) [55] to avoid catastrophic forgetting of earlier simulation time steps while training on later ones. To integrate with the streaming setup, we implemented this approach to continual learning as a separate component, called training buffer, between the streaming receiver and the training loop. This component holds two buffers: a now-buffer, which holds the $N_{\text{now}} = 10$ latest samples received. Each time new samples are received, they are prepended to the now-buffer and any element which would then exceed the buffer size is removed and added to the EP buffer. The EP buffer holds a maximum of $N_{\text{EP}} = 20$ elements. When new samples are to be added to the EP buffer when it is full, a randomly chosen item is removed. For a

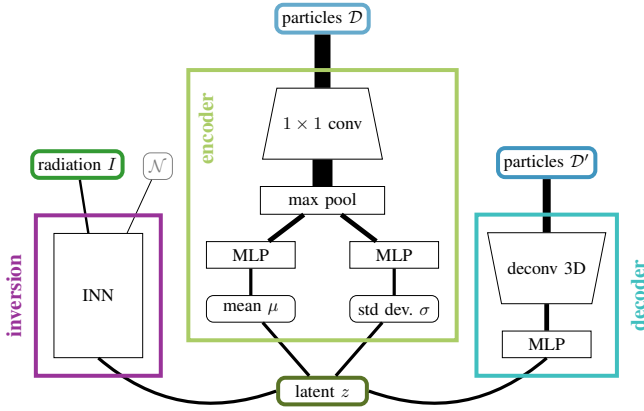


Fig. 7: Block-wise architecture of the ML model encompassing all three tasks summarized in Fig. 2 to allow in-transit training and regularize the pivotal latent space. Colored boxes correspond to the elements in Fig. 2. The black lines indicate information flow between blocks with their thicknesses illustrating the relative amounts of activations communicated. The combination of the encoder and decoder blocks constitute the VAE portion of the model.

single iteration of the training loop, a batch of data is requested from the training buffer. This batch constitutes the *training batch*. It is generated by taking $n_{\text{now}} = 4$ random samples from the now-buffer and $n_{\text{EP}} = 4$ random samples from the EP buffer, yielding a training batch size of $n_{\text{now}} + n_{\text{EP}} = 8$. In order to increase training success, we perform n_{rep} iterations of the training loop per single time step from the data stream. For each iteration, a new training batch is generated from the now- and EP buffer.

Separating the EP schedule from the training loop via our training buffer allows us to control how many batches we iterate per sample time-step produced, as long as we have some leeway to stall the running simulation if need be. This is crucial to allow the optimizer some amount of exploration, which can only happen sequentially and hence a smaller number of training iterations cannot be compensated by the large batch sizes of data-parallel training.

For all training runs, we use the Adam optimizer [56] with $\beta_1 = 0.8$, $\beta_2 = 0.9$, $\epsilon = 1 \cdot 10^{-6}$ and an L^2 weight decay strength of $2 \cdot 10^{-5}$. For data parallel training we employ PyTorch’s Distributed Data Parallel (DDP) module with its N/RCCL backend. Learning rates are scaled following a square-root rule [57]. In order to accelerate learning with large batch sizes, we train layers belonging to the VAE at a learning rate higher by a factor m_{VAE} than that of the INN.

Technical Challenges: The main drawback of CD, used as the VAE’s reconstruction loss, is its lacking sensitivity to point density. It also fails to distinguish some point configurations [58]. Both of these problems are overcome by the earth mover’s distance (EMD) [59] loss, but at much higher computational cost¹. Still, a rather compute and memory efficient differentiable implementation of EMD is available in the geomloss python package [60], which, instead of relying

¹We observed about a $4\times$ increase in batch times when using EMD [60] vs. a simple implementation of CD.

entirely on PyTorch, internally uses the KeOps library [61], [62] for performance. Unfortunately, the KeOps library is implemented directly in CUDA, and thus cannot be used on AMD GPUs in Frontier. Hence, we were barred from employing EMD loss in our runs on Frontier. Perhaps the community needs a HIP version of the KeOps library.

D. Setup on ORNL Frontier system

While distributing nodes exclusively to either PICongPU or to the MLapp, *inter-node* setup in Fig. 3(c), is easier to achieve in Slurm (and this strategy would be supported by our flexible I/O solution), we decide to use the *intra-node* setup in Fig. 3(c) and share each compute node between PICongPU and the MLapp. This has the advantage that data exchange mostly needs not leave the node, but requires a more specific resource allocation: Each single compute node no longer runs homogeneous parallel sub-jobs, but has to locally assign resources to heterogeneous applications. For our setup, this local assignment gives 4 GCDs to PICongPU and 4 GCDs to MLapp. In openPMD and ADIOS2, each reader application decides on its own which remote datasets to load. Here, the distribution of loaded data regions (i. e. local blocks within the global dataset) is configured such that data is shared within node boundaries.

Due to the plugin-based structure of PICongPU, both the particle and radiation input required by MLapp are provided by distinct output plugins of PICongPU, meaning that two parallel data streams are opened between PICongPU and the MLapp. Each plugin prepares the current time step’s data and, upon having all data ready, ADIOS2 will gather the metadata, including remote read addresses, to parallel rank 0 and provide the time step to the reader. The reader performs remote reads to its liking and closes the time step, indicating to the writer that the data can now be dropped.

A unique and important requirement of the presented workflow is the ability to not only run but also scale on a large number of Frontier’s AMD MI250X GPUs. Our machine learning model is small enough to fit on a single GCD; therefore, parallel training of this model is done using data parallelism where copies of the model are distributed across GCDs with each copy of the model receiving different chunks of data to train on. Once each model computes its gradients, all the instances of the model must do a collective all-reduce communication to average the gradients. We expect the scaling of the workflow to critically depend on the optimization of this all-to-all communication in PyTorch DDP, since communication within the PICongPU simulation is only between next neighbors. We experienced a hard limit to scaling in our current setup: The all-to-all communication between PyTorch DDP ranks using the N/RCCL backend hits system limitations on the possible number of open sockets beyond 100 nodes. Potential options to circumvent this limit include using a libfabric backend for N/RCCL or using PyTorch DDP’s MPI backend. While the N/RCCL backend was able to support PyTorch up to the scale used in this study, we can already conclude that further extensive evaluation of the communication backends

within PyTorch will become mandatory to provide a stable base for our near future scaling studies on Frontier. This area of research appears to be still under development, to the best of our knowledge [63].

V. RESULTS

A. Weak-Scaling

When training any kind of statistical model, in our case a deep neural network, one has to ensure that for each characteristic of the domain one hopes to learn, there are sufficient examples available in the dataset. When the dataset is provided in-transit, redundancy must still be built into the setup, either by using a large simulation volume or running multiple independent simulations concurrently, to allow the network to learn repeated patterns of the simulations and thereby distinguish relevant domain features, such as physical relationships, from noise. For this reason, in this work, we focus on a weak-scaling study of the proposed pipeline, as we anticipate this to be the most likely use-case. To evaluate parallel scaling as well as learning scaling, we performed simulations with in-transit training from 8 up to 96 nodes. The lower limit of 8 nodes is set by physical size constraints of the simulation. Fig. 8 shows the weak scaling behavior of the pipeline on Frontier. We define efficiency as the ratio of runtime at a specific size over runtime of the smallest size. Before averaging the times per training batch, we removed outliers more than four standard-deviations from the mean, because on Frontier we observed single batches taking more than $100\times$ the mean time.

While ideal scaling should correspond to 100% efficiency across all sizes, communication overheads reduce efficiency in practice. Here, the efficiency of in-transit training reaches around 35% at 96 nodes. We attribute the low parallel efficiency to two main reasons: One of them is the inevitable all-to-all communication between PyTorch ranks that takes place to average the gradients during each backward pass and obtain a synchronized result on all ranks, which accounts for a deficit of $\sim 30\%$, which is still a respectable result achieved by overlapping computations and communication in PyTorch DDP. The other is the computation of the two MMD loss terms, which amount to matrix dot products with data distributed across all ranks. Due to torch not offering a distributed primitive and the matrices involved being relatively small, even at the largest achieved scale, we opted for a naive implementation which replicates work between nodes. The global communication required here² breaks the torch computational graph, i.e. synchronizes graph execution with host code at the invocation site. To our knowledge there is no high-level API available to stitch these operations into the graph to allow them to be executed asynchronously to both the host and each other, i.e. no enqueueing of host functions or events.

²torch.distributed.all_gather_into_tensor

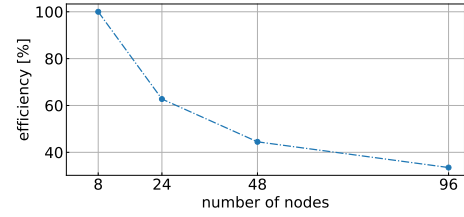


Fig. 8: Frontier weak scaling of the in-transit training from 32 to 384 GCDs (8 to 96 nodes). Measurements are single-batch times averaged over multiple runs and over iterations within runs after removal of $> 4\sigma$ outliers.

1) *Scaling Model Training*: The performed scaling runs, training with a batch size of $n_{\text{now}} + n_{\text{rep}} = 8$ per GCD, correspond to total batch sizes of 256 to 3072 on 32 to 384 GCDs, respectively.

In our scaling runs, we explored training from scratch at large scale, sampling up to $n_{\text{rep}} = 96$ batches per sample consumed from the stream and found learning success up to about $n_{\text{rep}} = 48$. We settled on a base-learning rate of $l_{\text{base}} = 1 \cdot 10^{-6}$, scaled according to the square-root scaling rule [57] depending on the actual number of GCDs. We observe a training speed up with larger batch sizes. That is, the increased learning rate overcompensates the training slow down due to larger batch sizes. Furthermore, it became evident that the three losses connected to the INN converged best at lower learning rates, while the VAE only found better minima at the highest learning rate, showing that separate learning rates l_{VAE} and l_{INN} of the encoder/decoder block and the inversion block, respectively, need to be applied at large scales.

Within the scope of this study, we have to conclude, that for in-transit training at very large batch sizes, hyper parameter studies do not transfer from small-scale experiments and thus have to be performed at scale. To enable in-transit learning at the scales we tested or beyond, comprehensive studies of the relations between the block learning rates l_{VAE} and l_{INN} , batch sizes, and maybe even loss weights in Eq. (1) have to be performed. Exploring this parameter space for the large scale training requires the full study to be systematically performed at these scales (up to 384 GCDs), either by employing a streamed simulation or the same training data stored on disk. We argue, that the latter is challenging at scale due to the lack of disk capacity and bandwidth.

B. Quantifying the predictive capabilities of the machine learning method

To evaluate the performance of the trained model, we invert the radiation spectra back to the original momentum distribution, focusing on the momentum component p_x in the following discussion (see Fig. 9). As this inversion is an unsolved problem in physics, we do not expect good agreement, but would be satisfied with partial reconstruction of the distribution.

Given spectra from the bulk of the plasma, the model reconstructs the momentum distribution quite well (blue and red Fig. 9(c)). The mean of the predicted momentum agrees

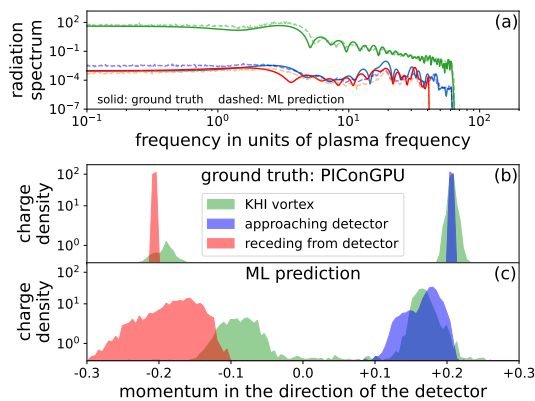


Fig. 9: Comparing the ground truth data from PIConGPU with the prediction of the ML model on a selected example sub-volume. Blue & red are undisturbed plasma streams approaching or receding from the detector, green depicts the KHI vortex regions. (a) radiation spectra, (b) ground truth and (c) predicted momentum distribution. The agreement is good enough to unambiguously classify the region of origin of the plasma instability based on the momentum distribution predicted by the radiation spectra.

with the distribution from PIConGPU (Fig. 9(b)). We also observe that the network learned a fundamental aspect of special relativity: the Doppler shift, to distinguish between plasma streams approaching and receding from the detector, since it reproduces the correct cutoff frequency when predicting spectra from particle data (Fig. 9(a) dotted lines).

The momentum prediction from the KHI shear surface was expected to be more difficult since particles from both directions cross in the shear surface, resulting in two separate and distinct particle populations. The ML reconstruction consistently predicts these two distinct populations. This is consistent with the interpretation, that the INN has learned unsupervised that the vortex region undergoes more acceleration and thus emits more intense radiation than the bulk of the plasma. However, the momentum prediction is less accurate: the mean of (one of) these populations often does not match the PIConGPU data (Fig. 9(b vs. c) green). We suspect that this is partly due to our choice of region boundaries on the shear surface, which results in a much lower sampling rate of one flow direction compared to the other, leading to a lower accuracy in predicting the mean of the lower peak of the momentum distribution. It is also possible, that this problem arises from the VAE’s decoder having difficulties reconstructing discontinuous distributions. Nevertheless, the successful prediction of shear regions indicates that the encoder extracts crucial features from the input data to recognize whether a region contains a vortex and encodes them in latent space.

Despite suboptimal reconstruction of vortex momenta, the ML prediction still allows to clearly identify KHI regions. Previous work on PC generation [64] observed that the latent space of an AE may contain more information than the decoder can reconstruct with satisfactory fidelity and that more sophisticated generative models, such as GANs or flows, can learn to produce more detailed reconstructions when conditioned on the same latent space.

While the prediction accuracy for the inversion from radiation to momentum is still limited, our workflow shows promising potential for automated learning of physical relationships from in-transit data of large-scale simulations and the identification of regions of instability is already a major step forward. This identification by the network may be obvious to a domain expert, but the *Artificial Scientist* learned the distinction unsupervised. The work has demonstrated, as a proof of principle, that it is possible to learn correlations from a physics simulation on-the-fly. **This is a promising first result towards large-scale in-transit learning for a non-steady state processes.**

Future work will explore more sophisticated network components such as (a) Deeper INNs with more powerful subnetwork architectures [44], (b) a wealth of more sophisticated PC decoder networks to generate higher-fidelity depictions of predicted particle distributions [64], and (c) more complex encoders architectures [51], ideally bringing contrastive learning approaches [65] to point clouds to learn better latent representations.

VI. CONCLUSION

By training a machine learning model on-the-fly on a PIConGPU simulation of the Kelvin-Helmholtz instability, where data is streamed via openPMD with ADIOS2, we demonstrate a realization of the *Artificial Scientist* solving an ill-posed inverse problem from plasma physics. This allows us to circumvent the lack of adequate disk capacity and bandwidth, often a bottleneck in large-scale systems, by enabling data to reside in-memory and be distributed via network between the nodes. Scientifically, this work also demonstrates as a proof of principle, that it is possible to learn correlations from a physics simulation on-the-fly. On full Frontier, we demonstrate streaming at scale using openPMD as well as performance studies at scale for general plasma physics.

REFERENCES

- [1] P.-T. Bremer, B. Spears, T. Gibbs, and M. Bussmann, “AI-Augmented Facilities: Bridging Experiment and Simulation with ML (Dagstuhl Seminar 23132),” *Dagstuhl Reports*, vol. 13, no. 3, pp. 106–131, 2023.
- [2] T. Zeng, Y. Zhu, and E. Y. Lam, “Deep learning for digital holography: a review,” *Opt. Express*, vol. 29, pp. 40572–40593, Nov 2021.
- [3] E. Kocer, T. W. Ko, and J. Behler, “Neural Network Potentials: A Concise Overview of Methods,” *Annual Review of Physical Chemistry*, vol. 73, no. Volume 73, 2022, pp. 163–186, 2022.
- [4] A. Döpp, C. Eberle, S. Howard, F. Irshad, J. Lin, and M. Streeter, “Data-driven Science and Machine Learning Methods in Laser-Plasma Physics,” *High Power Laser Science and Engineering*, pp. 1–50, 2023.
- [5] V. Belis, P. Odagiu, and T. K. Aarrestad, “Machine learning for anomaly detection in particle physics,” *Reviews in Physics*, vol. 12, p. 100091, 2024.
- [6] M. Bussmann, H. Burau, T. E. Cowan, A. Debus, A. Huebl, G. Juckeland, T. Kluge, W. E. Nagel, R. Pausch, F. Schmitt, U. Schramm, J. Schuchart, and R. Widera, “Radiative signatures of the relativistic Kelvin-Helmholtz instability,” in *SC ’13 Proceedings of the International Conference for High Performance Computing, Networking, Storage and Analysis*, pp. 5–1 – 5–12, 2013.
- [7] F. Meyer, B. Hernandez, R. Pausch, R. Widera, D. Groß, S. Baskakov, A. Huebl, G. Juckeland, J. Kelling, M. Leinhauser, D. Rogers, U. Schramm, K. Steiniger, S. Gumhold, J. Young, M. Bussmann, S. Chandrasekaran, and A. Debus, “Hardware-agnostic interactive exascale in situ visualization of particle-in-cell simulations,” in *Proceedings*

- of the Platform for Advanced Scientific Computing Conference, PASC '23, (New York, NY, USA), Association for Computing Machinery, 2023.
- [8] A. K. Sen, "Stability of Hydromagnetic Kelvin-Helmholtz Discontinuity," *Physics of Fluids*, vol. 6, no. 8, p. 1154, 1963.
 - [9] I. Goodfellow, Y. Bengio, and A. Courville, *Deep Learning*. MIT Press, 2016. <http://www.deeplearningbook.org>.
 - [10] H. M. Gomes, J. Read, A. Bifet, J. P. Barddal, and J. a. Gama, "Machine learning for streaming data: state of the art, challenges, and opportunities," *SIGKDD Explor. Newsl.*, vol. 21, p. 6–22, nov 2019.
 - [11] L. Wang, X. Zhang, H. Su, and J. Zhu, "A Comprehensive Survey of Continual Learning: Theory, Method and Application," 2024.
 - [12] A. Huebl, R. Widera, F. Schmitt, A. Matthes, N. Podhorszki, J. Y. Choi, S. Klasky, and M. Bussmann, "On the scalability of data reduction techniques in current and upcoming hpc systems from an application perspective," in *High Performance Computing* (J. M. Kunkel, R. Yokota, M. Tauber, and J. Shalf, eds.), (Cham), pp. 15–29, Springer International Publishing, 2017.
 - [13] L. Wan, A. Huebl, J. Gu, F. Poeschel, A. Gainaru, R. Wang, J. Chen, X. Liang, D. Ganyushin, T. Munson, I. Foster, J.-L. Vay, N. Podhorszki, K. Wu, and S. Klasky, "Improving i/o performance for exascale applications through online data layout reorganization," *IEEE Transactions on Parallel and Distributed Systems*, vol. 33, no. 4, pp. 878–890, 2022.
 - [14] F. Poeschel, J. E. W. F. Godoy, N. Podhorszki, S. Klasky, G. Eisenhauer, P. E. Davis, L. Wan, A. Gainaru, J. Gu, F. Koller, R. Widera, M. Bussmann, and A. Huebl, "Transitioning from file-based hpc workflows to streaming data pipelines with openpmd and adios2," in *Driving Scientific and Engineering Discoveries Through the Integration of Experiment, Big Data, and Modeling and Simulation* (J. Nichols, A. B. Maccabe, J. Nutaro, S. Pophale, P. Devineni, T. Ahearn, and B. Verastegui, eds.), (Cham), pp. 99–118, Springer International Publishing, 2022.
 - [15] OLCF, "Frontier." <https://www.olcf.ornl.gov/frontier/>, 2024. [Online; accessed 09-October-2024].
 - [16] "PUNCH4NFDI Use case class 5: real-time challenges, data irreversibility," 2024.
 - [17] "PyTorch Distributed Data Parallel Documentaion." <https://pytorch.org/docs/2.0/notes/ddp.html>.
 - [18] P. Delamere, R. Wilson, and A. Masters, "Kelvin-helmholtz instability at saturn's magnetopause: Hybrid simulations," *Journal of Geophysical Research: Space Physics*, vol. 116, no. A10, 2011.
 - [19] A. Casner, "Recent progress in quantifying hydrodynamics instabilities and turbulence in inertial confinement fusion and high-energy-density experiments," *Philosophical Transactions of the Royal Society A*, vol. 379, no. 2189, p. 20200021, 2021.
 - [20] J. D. Sadler, S. Green, S. Li, Y. Zhou, K. A. Flippo, and H. Li, "Faster ablative kelvin-helmholtz instability growth in a magnetic field," *Physics of Plasmas*, vol. 29, no. 5, 2022.
 - [21] T. Grismayer, E. P. Alves, R. a. Fonseca, and L. O. Silva, "dc-magnetic-field generation in unmagnetized shear flows," *Physical Review Letters*, vol. 111, p. 015005, 7 2013.
 - [22] E. P. Alves, T. Grismayer, S. F. Martins, F. Fiúza, R. a. Fonseca, and L. O. Silva, "Large-Scale Magnetic Field Generation Via the Kinetic Kelvin-Helmholtz Instability in Unmagnetized Scenarios," *The Astrophysical Journal Letters*, vol. 746, no. 2, p. L14, 2012.
 - [23] R. Pausch, M. Bussmann, A. Huebl, U. Schramm, K. Steiniger, R. Widera, and A. Debus, "Identifying the linear phase of the relativistic kelvin-helmholtz instability and measuring its growth rate via radiation," *Physical Review E*, vol. 96, p. 013316, 7 2017.
 - [24] H. Burau, R. Widera, W. Hönig, G. Juckeland, A. Debus, T. Kluge, U. Schramm, T. E. Cowan, R. Sauerbrey, and M. Bussmann, "PICongPU: A fully relativistic particle-in-cell code for a GPU cluster," *IEEE Transactions on Plasma Science*, vol. 38, no. 10 PART 2, pp. 2831–2839, 2010.
 - [25] E. Zenker, B. Worpitz, R. Widera, A. Huebl, G. Juckeland, A. Knüpfer, W. E. Nagel, and M. Bussmann, "Alpaka – an abstraction library for parallel kernel acceleration," in *2016 IEEE International Parallel and Distributed Processing Symposium Workshops (IPDPSW)*, pp. 631–640, 5 2016.
 - [26] R. W. Hockney and J. W. Eastwood, *Computer simulation using particles*. Bristol and New York: Adam Hilger - IOP Publishing Ltd, 1988.
 - [27] "TWEAC test-case PICongPU." <https://github.com/ComputationalRadiationPhysics/picongpu/tree/dev/share/picongpu/benchmarks/TWEAC-FOM>, 2023.
 - [28] "Frontier User Guide: System Overview." https://docs.olcf.ornl.gov/systems/frontier_user_guide.html#frontier-compute-node. [Online; accessed 2024-04-02].
 - [29] W. Hönig, F. Schmitt, R. Widera, H. Burau, G. Juckeland, M. S. Müller, and M. Bussmann, "A Generic Approach for Developing Highly Scalable Particle-Mesh Codes for GPUs," *SAHPC.–2010*, 2010.
 - [30] "libPMacc." <https://github.com/ComputationalRadiationPhysics/picongpu/tree/dev/include/pmacc>, 2023.
 - [31] F. Koller, F. Poeschel, J. Gu, and A. Huebl, "openpmd-api: C++ & python api for scientific i/o with openpmd," 2018.
 - [32] A. Huebl, R. Lehe, J.-L. Vay, D. P. Grote, I. Sbalzarini, S. Kuschel, D. Sagan, F. Pérez, F. Koller, and M. Bussmann, "openPMD 1.1.0: Base paths for mesh- and particle- only files and updated attributes," Feb. 2018.
 - [33] W. F. Godoy, N. Podhorszki, R. Wang, C. Atkins, G. Eisenhauer, J. Gu, P. Davis, J. Choi, K. Germaschewski, K. Huck, A. Huebl, M. Kim, J. Kress, T. Kurc, Q. Liu, J. Logan, K. Mehta, G. Ostrouchov, M. Parashar, F. Poeschel, D. Pugmire, E. Suchyta, K. Takahashi, N. Thompson, S. Tsutsumi, L. Wan, M. Wolf, K. Wu, and S. Klasky, "Adios 2: The adaptable input output system. a framework for high-performance data management," *SoftwareX*, vol. 12, p. 100561, 2020.
 - [34] R. Pausch, A. Debus, R. Widera, K. Steiniger, A. Huebl, H. Burau, M. Bussmann, and U. Schramm, "How to test and verify radiation diagnostics simulations within particle-in-cell frameworks," *Nuclear Instruments and Methods in Physics Research Section A: Accelerators, Spectrometers, Detectors and Associated Equipment*, vol. 740, pp. 250–256, 3 2014.
 - [35] J. D. Jackson, *Classical Electrodynamics*. New York: John Wiley and Sons, Inc., third ed., 1998.
 - [36] R. Pausch, A. Debus, A. Huebl, U. Schramm, K. Steiniger, R. Widera, and M. Bussmann, "Quantitatively consistent computation of coherent and incoherent radiation in particle-in-cell codes - a general form factor formalism for macro-particles," *Nuclear Instruments and Methods in Physics Research Section A: Accelerators, Spectrometers, Detectors and Associated Equipment*, vol. 909, pp. 419–422, 11 2018. in press, corrected proof published online.
 - [37] R. Pausch, H. Burau, M. Bussmann, J. Couperus, T. E. Cowan, A. Debus, A. Huebl, A. Irman, A. Köhler, U. Schramm, K. Steiniger, and R. Widera, "Computing Angularly-Resolved Far-Field Emission Spectra In Particle-In-Cell Codes Using GPUs," in *Proceedings of IPAC2014*, pp. 761–764, 2014.
 - [38] "Overview on projects around openPMD." <https://github.com/openPMD/openPMD-projects>, 2024. [Online; accessed 2024-04-02].
 - [39] A. Gainaru, L. Wan, R. Wang, E. Suchyta, J. Chen, N. Podhorszki, J. Kress, D. Pugmire, and S. Klasky, "Understanding the impact of data staging for coupled scientific workflows," *IEEE Transactions on Parallel and Distributed Systems*, vol. 33, no. 12, pp. 4134–4147, 2022.
 - [40] G. Eisenhauer, N. Podhorszki, A. Gainaru, S. Klasky, P. E. Davis, M. Parashar, M. Wolf, E. Suchyta, E. Fredj, V. Bolea, F. Pöschel, K. Steiniger, M. Bussmann, R. Pausch, and S. Chandrasekaran, "Streaming data in hpc workflows using adios," 2024.
 - [41] "Open Fabric Interfaces." <https://github.com/ofiwg/libfabric/>. [GitHub repository; accessed 2024-04-02].
 - [42] "OLCF announces storage specifications for Frontier Exascale System." <https://www.olcf.ornl.gov/2021/05/20/olcf-announces-storage-specifications-for-frontier-exascale-system/>, 2021. [Online; accessed 2024-04-02].
 - [43] Y. Gal and Z. Ghahramani, "Dropout as a Bayesian Approximation: Representing Model Uncertainty in Deep Learning," 2016.
 - [44] L. Dinh, J. Sohl-Dickstein, and S. Bengio, "Density estimation using Real NVP," *CoRR*, vol. abs/1605.08803, 2016.
 - [45] Y. Lu and B. Huang, "Structured Output Learning with Conditional Generative Flows," 2020.
 - [46] L. Ardizzone, J. Kruse, S. J. Wirkert, D. Rahner, E. W. Pellegrini, R. S. Klessen, L. Maier-Hein, C. Rother, and U. Köthe, "Analyzing Inverse Problems with Invertible Neural Networks," *CoRR*, vol. abs/1808.04730, 2018.
 - [47] E. Tabak and E. Vanden-Eijnden, "Density estimation by dual ascent of the log-likelihood," *Communications in Mathematical Sciences*, vol. 8, no. 1, pp. 217–233, 2010.
 - [48] E. G. Tabak and C. V. Turner, "A Family of Nonparametric Density Estimation Algorithms," *Communications on Pure and Applied Mathematics*, vol. 66, no. 2, pp. 145–164, 2013.

- [49] L. Dinh, D. Krueger, and Y. Bengio, "NICE: Non-linear Independent Components Estimation," 2015.
- [50] L. Kong, P. Rajak, and S. Shakeri, "Generative Models for 3D Point Clouds," 2023.
- [51] C. R. Qi, H. Su, K. Mo, and L. J. Guibas, "PointNet: Deep Learning on Point Sets for 3D Classification and Segmentation," 2017.
- [52] D. P. Kingma and P. Dhariwal, "Glow: Generative Flow with Invertible 1x1 Convolutions," in *Advances in Neural Information Processing Systems* (S. Bengio, H. Wallach, H. Larochelle, K. Grauman, N. Cesa-Bianchi, and R. Garnett, eds.), vol. 31, Curran Associates, Inc., 2018.
- [53] H. Fan, H. Su, and L. Guibas, "A Point Set Generation Network for 3D Object Reconstruction from a Single Image," 2016.
- [54] D. P. Kingma and M. Welling, "Auto-Encoding Variational Bayes," 2013.
- [55] A. Chaudhry, M. Rohrbach, M. Elhoseiny, T. Ajanthan, P. K. Dokania, P. H. S. Torr, and M. Ranzato, "On tiny episodic memories in continual learning," *arXiv: Learning*, 2019.
- [56] D. P. Kingma and J. Ba, "Adam: A Method for Stochastic Optimization," 2017.
- [57] A. Krizhevsky, "One weird trick for parallelizing convolutional neural networks," 2014.
- [58] P. Achlioptas, O. Diamanti, I. Mitliagkas, and L. Guibas, "Learning Representations and Generative Models for 3D Point Clouds," in *Proceedings of the 35th International Conference on Machine Learning* (J. Dy and A. Krause, eds.), vol. 80 of *Proceedings of Machine Learning Research*, pp. 40–49, PMLR, 10–15 Jul 2018.
- [59] Y. Rubner, C. Tomasi, and L. J. Guibas, "The Earth Mover's Distance as a Metric for Image Retrieval," *International Journal of Computer Vision*, vol. 40, pp. 99–121, Nov 2000.
- [60] J. Feydy, T. Séjourné, F.-X. Vialard, S.-i. Amari, A. Trounev, and G. Peyré, "Interpolating between Optimal Transport and MMD using Sinkhorn Divergences," in *The 22nd International Conference on Artificial Intelligence and Statistics*, pp. 2681–2690, 2019.
- [61] B. Charlier, J. Feydy, J. A. Glaunès, F.-D. Collin, and G. Durif, "Kernel Operations on the GPU, with Autodiff, without Memory Overflows," *Journal of Machine Learning Research*, vol. 22, no. 74, pp. 1–6, 2021.
- [62] J. Feydy, J. Glaunès, B. Charlier, and M. Bronstein, "Fast geometric learning with symbolic matrices," *Advances in Neural Information Processing Systems*, vol. 33, 2020.
- [63] S. Dash, I. Lyngaas, J. Yin, X. Wang, R. Egele, G. Cong, F. Wang, and P. Balaprakash, "Optimizing distributed training on frontier for large language models," 2023.
- [64] P. Achlioptas, O. Diamanti, I. Mitliagkas, and L. Guibas, "Learning representations and generative models for 3D point clouds," in *Proceedings of the 35th International Conference on Machine Learning* (J. Dy and A. Krause, eds.), vol. 80 of *Proceedings of Machine Learning Research*, pp. 40–49, PMLR, 10–15 Jul 2018.
- [65] M. Caron, H. Touvron, I. Misra, H. Jégou, J. Mairal, P. Bojanowski, and A. Joulin, "Emerging Properties in Self-Supervised Vision Transformers," 2021.